Review—A Pollutant Gas Sensor Based On Fe3 O4 Nanostructures: A Review

by Mochamad Zakki Fahmi

Submission date: 01-Sep-2021 08:59PM (UTC+0800)
Submission ID: 1639432387
File name: A38-Review_A_Pollutant_Gas_Sensor_Based_On_Fe3o4.pdf (1.89M)
Word count: 10421
Character count: 52215

Journal of The Electrochemical Society

Review—A Pollutant Gas Sensor Based On Fe_3O_4 Nanostructures: A Review

Journal of The Electrochemical Society, 2021 168 027510
1945-7111/2021/168(2)/027510/12/$40.00 © 2021 The Electrochemical Society ("ECS"). Published on behalf of ECS by IOP Publishing Limited

Review—A Pollutant Gas Sensor Based On Fe_3O_4 Nanostructures: A Review

Juliandi Siregar,[1,2] Ni Luh Wulan Septiani,[3] Syauqi Abdurrahman Abrori,[3] Kerista Sebayang,[1,z] Irzaman,[4] Mochammad Zakki Fahmi,[5] Syahrul Humaidi,[1] Timbangen Sembiring,[1] Kurnia Sembiring,[1] and Brian Yuliarto[3,6,z]

[1]*Department of Physics, FMIPA, Universitas Sumatera Utara, Jl. Bioteknologi I Kampus USU, Medan 20155, Indonesia*
[2]*Universitas Muslim Nusantara Al Washliyah, Jl. Garu II A No. 93, Medan Amplas, Kota Medan, Indonesia*
[3]*Advanced Functional Materials Research Group, Faculty of Industrial Technology, Institut Teknologi Bandung, Indonesia*
[4]*Department of Physics, Faculty of Mathematics and Natural Sciences, Bogor Agricultural University of Indonesia, Bogor, Indonesia*
[5]*Department of Chemistry, Universitas Airlangga, Surabaya, Indonesia*
[6]*Research Center of Nanosciences and Nanotechnology, Institut Teknologi Bandung, Indonesia*

Magnetite (Fe_3O_4) nanostructures and their modifications with other materials show proper characteristics to be implemented as a sensing material. This paper provides a brief review of the application of the Fe_3O_4 nanostructures and their modifications as sensitive material for pollutant gas sensors. Several studies were highlighted to explain the past-to-present progress of materials development. Various synthesis procedures of the materials were also clearly explained. The application of pure Fe_3O_4 nanostructures and their modification as sensitive materials in gas sensor devices to detect toxic gases is the main section of this paper. Last, the future prospects section summarized the materials' development and provided a suggestion for future development.
 [DOI: 10.1149/1945-7111/abd928]

Manuscript submitted September 23, 2020; revised manuscript received December 4, 2020. Published February 10, 2021.

For many years, various transition metal oxides such as zinc oxide (ZnO),[1–5] tin oxide (SnO_2),[6–8], and iron oxide,[9–13] have been investigated in a wide field such as catalyst sensor, supercapacitor, medicine, battery, and so on. Among the oxides, iron oxide has attracted many researchers due to its attractive properties. The oxide has three phases in nature, namely Magnetite (Fe_3O_4),[14,15] maghemite (γ-Fe_2O_3),[16–19], and hematite (α-Fe_2O_3).[18,19] Both magnetite and maghemite are ferrimagnetic materials with magnetic behavior under Curie temperature exposure, while hematite has paramagnetic properties. As a ferrimagnetic material, Fe_3O_4 is considered an attractive material due to its unique physical and chemical properties and its half-metal property.[20,21] With some of these exciting characteristics, several studies have succeeded in implemented Fe_3O_4 nanoparticles as an active material to kill pathogenic bacteria[22,23]; in the biomedical dan bioengineering field[24,25]; gas sensor[26] biomaterials[27,28]; and bioseparation.[29]

Fe_3O_4 has the most potent magnetism among the other iron oxide phases. The ideal formula of magnetite is $Fe^{2+}Fe_2^{3+}O_4$. The main details of its structure were first studied in 1915 using X-ray Diffraction, and one of the first crystal structures evaluated by Bragg analysis. Magnetite has an inverse-spinel structure that crystallizes in the isometric space group Fd3m.[30] The unit cell of magnetite has a structural parameter equal to 0.8396 nm and contains 32 close-packed oxygen ions forming a face-centered cubic lattice and 24 iron cations occupying the interstitial sites. Eight of the Fe^{3+} cations occupy all eight of the tetrahedral sites.[9,31,32] Meanwhile, the remaining Fe^{3+} ions and Fe^{2+} ions are distributed randomly toward the octahedral sites. A view of the magnetite structure in Fig. 1 shows layers of oxygen atoms alternating with layers of iron cations.

The iron atom has four unpaired electrons in its 3d orbitals, resulting in an intense magnetic moment. Hematite itself has a ferrimagnetic at room temperature.[33] A ferrimagnetic material is a material that has two types of atoms with opposing magnetic moments, as in antiferromagnetism, but the opposing moments are unequal, and a spontaneous magnetization remains. This phenomenon happens when the material consists of different ions; in this case, Fe^{2+} and Fe^{3+}. The ordered arrangement of magnetic moments decreases with increasing temperature due to thermal fluctuations of the individual moments. Beyond the Curie temperature, the material becomes disordered and loses its magnetization. Curie temperature for hematite is 850 K. Hematite also displays superparamagnetic behavior at room temperature when its particles are smaller than 6 nm,[34,35] i.e., can be magnetized under an external magnetic field and will lose the magnetization when removing the field. This lack of net magnetization in the absence of field allows Fe_3O_4 nanoparticles to avoid magnetic aggregation, a common problem with magnetic particles significantly.

The electronic properties, as well as magnetic properties of Fe_3O_4, has been reported to be able to be exploited as a gas sensor. The relatively low bandgap of the material, i.e., 0.1 eV, makes them have relatively higher conductivity than other metal oxides. As a magnetic material, the interaction between the gas and the magnetite's surface will cause changes in the magnetic properties and affect the gas sensor's performance, such as sensitivity, selectivity, response time, and recovery time.[36,37] Gas adsorption on the surface of the material will change the surface state by introducing spin polarization, destroying the surface structure's symmetry, or disturbing the surface strain.[37,38] Study by Kumar et al. reported that small particle size supported by high magnetic saturation and low coercivity would result in high sensor performance.[39] as the best of our knowledge, the use of changes in magnetic properties has not been widely explored in magnetite material. It is an open opportunity for further development.

Furthermore, its characteristics allow it to be exploited either as a supporting material or a host material for gas sensors. This report contains a brief review of the gas sensor based on Fe_3O_4 and its modifications. This review is divided into five sections. The first section is an introduction containing brief information on Fe_3O_4 characteristics. The second section discusses several Fe_3O_4 preparation methods. The third section contains the discussion of the development of Fe_3O_4 as an active material for gas sensors. The Fourth section discusses the possible sensing mechanism occurring on the Fe_3O_4 surface and its modifications. Finally, the fifth section shows the future perspective of the development of sensor gas based on Fe_3O_4. This review is expected to contribute to the effort for the high performance of Fe_3O_4 based gas sensors in the future.

Fe_3O_4 Nanostructures Preparation Methods

In gas sensor materials, the synthesis strategies do not directly relate to the gas sensor performances. However, the strategy will affect the size and shape of the resulting Fe_3O_4 nanoparticles, where

[z]E-mail: keristasebayang@usu.ac.id; brian@tf.itb.ac.id

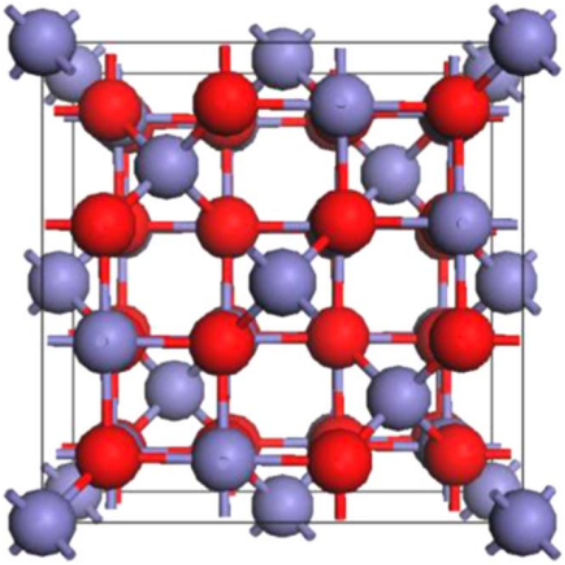

Figure 1. The crystal structure of magnetite (Fe_3O_4) in its cubic F3dm phase. Reprinted from publication[35] with permission from Taylor & Francis.

those parameters determine specific surface area and porosity. As we have known, the gas sensor is a surface phenomenon; the higher the surface area and porosity, the higher the performance. The effort to achieve the high performances of gas sensors based on Fe_3O_4 could be started by choosing a synthesis strategy to get the nanoscale particles with good dispersion and a high degree of uniformity. In other ways, one can choose or modify synthesis strategy to develop one dimensional, two dimensional, or hierarchical three dimensional of Fe_3O_4. This section will review some magnetite preparation methods based on several reports in the past five years.

Coprecipitation method.—Coprecipitation is a wet chemical method used to synthesize nanoparticles. Nanoparticles produced from the coprecipitation method are normally poly dispersive with spherical morphology. In general, the yield of Fe_3O_4 nanoparticles produced is the most compared to other synthesis methods. The disadvantages of the coprecipitation method are that the nanoparticles are easily agglomerated, so surface functionalization or capping agents are needed to overcome this problem. This method used precursors in the form of anhydrous metal salts as a source of metal cations and wet hydroxide compounds such as NaOH and KOH as co-precipitants. The coprecipitation method is considered the most straightforward method because it does not require high-temperature treatment ($T < 120$ °C) for the synthesis of Fe_3O_4 particles. There are three main steps in the Fe_3O_4 synthesis through the coprecipitation method. First, the preparation of the precursor (metal salt solution). Second, the formation of nanoparticles through alkaline reaction. Third, the process of washing the Fe_3O_4 nanoparticle slurry and drying process to get the brownish powder. Using this method, magnetite nanoparticles were prepared with iron sand used as an iron source in our previous work.[14] Fe^{2+}/Fe^{3+} solution was obtained by dissolving iron sand in 12 M HCl at ±70 °C. Polyethylene glycol (PEG) was dissolved in the solution in order to modify the morphology. The co-precipitant of NH_4OH was then dropped slowly under ultrasonication condition until the pH of 10 was obtained. The precipitated product was then washed several times to get a neutral slurry product. The magnetite powder was collected after the drying process. The resulting morphologies were found to depend on the amount of PEG that was added, as seen in Fig. 2.

In the magnetite preparation, one should note that the Fe_3O_4 phase was formed by a combination between Fe^{2+} and Fe^{3+} at a specific ratio. Hence two iron sources should be employed in the preparation process. Fe_3O_4 nanoparticles were successfully synthesized using a combination of $FeCl_3.6H_2O$ and $FeCl_2.4H_2O$ with a ratio of 2:1 in the deoxygenated distilled water.[40] In this case, a certain amount of ammonia was added rapidly under ultrasonic irradiation at 40 °C. Moreover, N_2 gas was also flown to the solution during the process. The black precipitate was then collected using magnetic decantation and was dried at 70 °C after the washing process. The formation of spherical particles with a size of 10 nm was obtained by this method. The ultrasound that interacts with the liquid medium is believed can inhibit particle growth. Garcia's group used $FeCl_3$ as a Fe^{3+} source and $FeSO_4$ as a Fe^{2+} source.[41] Their works also used distilled water medium and NH_4OH as precipitant. However, unlike the other works mentioned before, the final pH was kept at seven or neutral. They proposed to coat the resulted nanoparticles with two different sodium citrate agents and silica to induce surface passivation. Based on their result, the average size of particles decreases from 45.8 nm to 35.7 nm and 38.6, for sodium citrate and silica coating, respectively, indicating the better action of sodium citrate in growth prevention.

Another route called the reduction-precipitation method for the preparation of Fe_3O_4 nanoparticles was proposed by Cao et al.[42] The

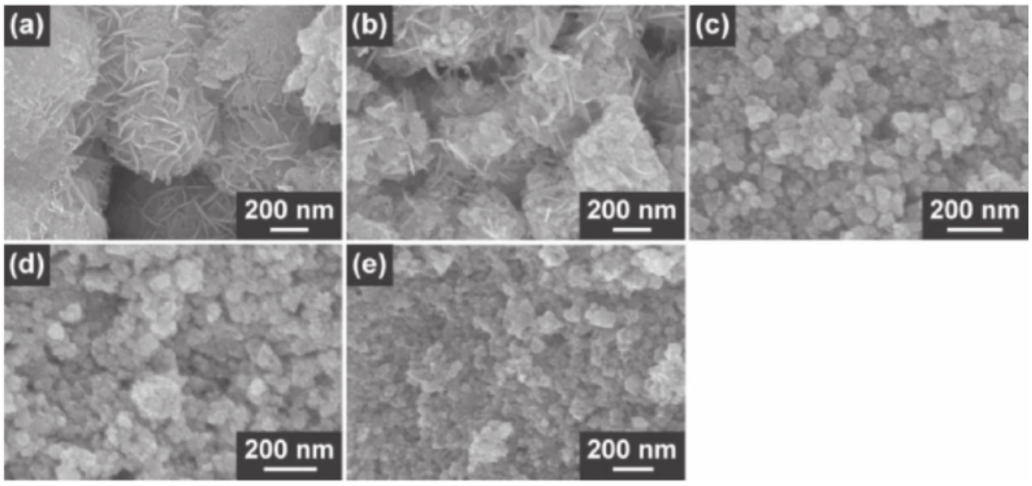

Figure 2. The magnetite particles synthesized by co-precipitation method with the presence of PEG of 5% (a), 10% (b), 15% (c), 20% (d), and 25% (e). Reprinted from publication[14] with permission from The Chemical Society of Japan.

preparation was succeeded with chitosan assist as a chelating agent, sodium sulfate as a reducing agent, and ammonia as a precipitant. Fe^{3+} that was chelated by the chitosan chain was partially reduced by sodium sulfate at the first stage. This process was completed by only adding the reducing agent to the mixture of $FeCl_3$ and chitosan solution at room temperature. The Fe_3O_4 nanoparticles of Fe_3O_4 with the size in the range of 5–8 nm were formed after the ammonia was added to the final solution. Another group also prepared the magnetite nanoparticles with a similar method but chose pregnant leach solution (PLS) of iron ore as an iron source.[43] To obtain the PLS, the iron ore was firstly ball-milled and then leached at 85 °C using H_2SO_4(5 M)/NaCl (2 M) for 120 min to decrease impurities. The resulting PLS was reduced partially by adding sodium thiosulfate, and the Fe_3O_4 precipitate was obtained after the addition of the ammonia solution.

From the studies explained above, it can be seen that the synthesis of the Fe_3O_4 nanoparticles was successfully carried out through the coprecipitation method. The synthesis of Fe_3O_4 was carried out at pH = 7–10 and at relatively low temperature to produce a precipitate that formed solid black and can be decanted by magnetism. Pure Fe_3O_4 nanoparticles are often found to be poor stability and dispersion characteristics. It is necessary to modify the synthesis process and choose the right procedure to produce Fe_3O_4, which is soluble and compatible so that Fe_3O_4 can be used for various applications.

The thermal decomposition method.—The thermal decomposition method is a synthesis method that uses a high-temperature environment (T > 200 °C) to obtain Fe_3O_4 nanoparticles with a tiny particle size distribution and a high degree of crystallinity. There are two types of precursors involved in this method, Fe metal precursors in organometallic compounds and organic surfactants. Organic surfactants usually act as a stabilizer to prevent particle aggregation. Organic surfactants such as oleic acid,[44,45] oleylamine,[46] or trioctylamine,[47] have been reported could stabilize the nanoparticles and result in mono diversity. Shape, morphology, particle size distribution, and the degree of crystallinity of Fe_3O_4 particles produced through this method are highly dependent on several synthesis parameters, such as temperature, duration of the synthesis, solvent, and surfactant used. The thermal decomposition method's disadvantages require high-temperature treatment during the synthesis process and involving expensive organometallic precursors.

Amara et al. produced monodisperse Fe_3O_4 using thermal decomposition of organometallic iron.[44] The iron complex was prepared by refluxing tri-iron dodecacarbonyl in diethylene glycol diethyl ether in the presence of oleic acid at 120 °C for 12 h and 165 °C for another two hours. The black to the brown product was heated at three different temperature of 300 °C, 700 °C, and 900 °C for 2.5 h under Argon atmosphere. They found that the formation of Fe_3O_4 with the size of 5.41 nm occurred at an annealing temperature of 300 °C. The increase of the particle size and aggregation were observed when the annealing temperature rose to 700 °C and 900 °C, as seen in Fig. 3. At a temperature higher than 300 °C, oleic acid disappeared and caused the agglomeration. A new route to prepare Fe_3O_4 nanoparticles was proposed by Glasgow et al.[47] The nanoparticles were transformed from iron oleate via thermal decomposition. Iron oleate was prepared by mixing sodium oleate and iron chloride hexahydrate in the mixture of ethanol, hexane, and deionized water solution at 70 °C for four hours. After cooling down, the resulted solution was washed using a separatory funnel; the solution was evaporated to get solid products. In order to get Fe_3O_4, the resulted iron oleate was mixed with oleic acid and trioctylamin. The solution the transferred to the flask under nitrogen flow. In their design, the solution was pumped into the coil that was connected with a salt bath. The hot plate heated the bath at 320 °C, and the flow was kept at the rate of 0.175 ml min^{-1}. Their study found that the ratio of iron oleate/oleic acid affects the size of particles. The best ratio was found to be 2:1, which result in particles with a size of 6.97 nm.

Synthesis of Fe_3O_4 through the sol-gel method.—The sol-gel is a synthesis method that is generally used to produce powder types of nanomaterials. The term sol-gel is derived from two words. The "sol" refers to a colloidal solution of precursors that will be used as starting material for the synthesis of Fe_3O_4 particles, and the "gel" refers to the form of the polymeric network of the final product of nanoparticles synthesized.[48,49] This method contains two main stages, hydrolysis, and condensation. Many synthesis parameters such as hydrolysis rate, condensation of metal oxides, pH, temperature, stirring method, oxidation rate, concentration, and precursor properties must be considered. The sol-gel method has several disadvantages, such as producing much alcohol during the calcination process, requiring additional heat treatment at high temperatures, and produce nanoparticles with high permeability and weak nanoparticle bonding powder characteristics. In the case of magnetite materials, several reports demonstrate the formation of nanoparticles using this method. For instance, Hu et al. produced 3–20 nm of magnetite using the sol-gel explosion-assisted method.[50] In their work, the dry gel was prepared by reacting ferric nitrate, citric acid, and ammonia at 68 °C, followed by evaporation at 95 °C. Citric acid as an explosion agent mixed with the dry gel at a specific ratio then is transferred to the autoclave system to complete carbothermal reaction at 450 °C. The gas generated during the explosion is believed to deposit on the nanoparticles' surface and induce a steric hindrance effect.

Nearly monodisperse Fe_3O_4 nanoparticles with an average diameter of 4.9 nm were demonstrated by Cui et al.[51] They offered the sol-gel route without the calcination process. In their typical procedure, $FeCl_2$ was used as an iron source, and propylene oxide was used as a Fe-OH generator. Both precursors were reacted in ethanol medium at 78 °C for 30 min, and the resulted paste-like gel of Fe_3O_4 was dried at room temperature. They also reported that other iron oxide phases like α-Fe_2O_3 and γ-Fe_2O_3 were formed if the drying process is performed at a higher temperature. Another sol-gel approach was demonstrated by Sciancalepore et al., where like the one reported by Cui et al., this approach followed a non-hydrolytic route. Iron (III)-acetylacetonate and 2-ethyl-1,3-hexanediol were used as a precursor and reactive solvent, respectively.[52] The formation of nanoparticles was induced by the reaction of $Fe(AcAc)_3$ and 2-ethyl-1,3-hexanediol (HD) at 200 °C for 48 h. They found that the precursor to solvent ratio affects the size and morphology of resulting particles. At a low ratio, small and nearly spherical particle formation were occurred, while at a high ratio, anisotropic crystal growth and more extensive particle formation have occurred. Figures 4a and 4b show the resulting Fe_3O_4 nanoparticles with $Fe(AcAc)_3$:HD ratio of 0.11 and 0.22, respectively.

Synthesis of Fe_3O_4 through the hydrothermal/solvothermal method.—Hydrothermal or solvothermal is a kind of wet synthesis that involves temperature and pressure in preparing the nanostructure of materials. Usually, the pressure in the sealed chemical reaction is controlled by temperature.[53,54] Qu et al. performed a solvothermal reaction to prepare a microsphere of Fe_3O_4.[55] A solution contains $FeSO_4.7H_2O$, sodium acetate, and trisodium citrate in ethanol is prepared and transferred to a Teflon-lined stainless autoclave. The solution is subjected to 160 °C for 5 h. The magnetite microsphere with diameter size in the range of 600–1000 nm is produced after calcination of solvothermal product at 300 °C for 2 h. A relatively low temperature hydrothermal was demonstrated by Jesus et al.[56] The combination of $FeCl_3$ and $FeCl_2$ with a specific ratio were dissolved in distilled water in the presence of sucrose as a chelating agent. Sodium hydroxide was employed as a pH controller with an acidity level target is 12. The mixture solution is subjected to hydrothermal reaction at 45 °C for 3 h. The particles with a size of less than 10 nm were produced using this strategy. Sucrose was also employed by Gao et al. to prepare hollow Fe_3O_4 nanoparticles, as seen in Figs. 4c, 4d.[57] They used the mixture of $FeSO_4.7H_2O$, urea, sodium hydroxide, PEG-200, and sucrose are used as a precursor and was subjected to solvothermal reaction at 200 °C for 10 h. In their

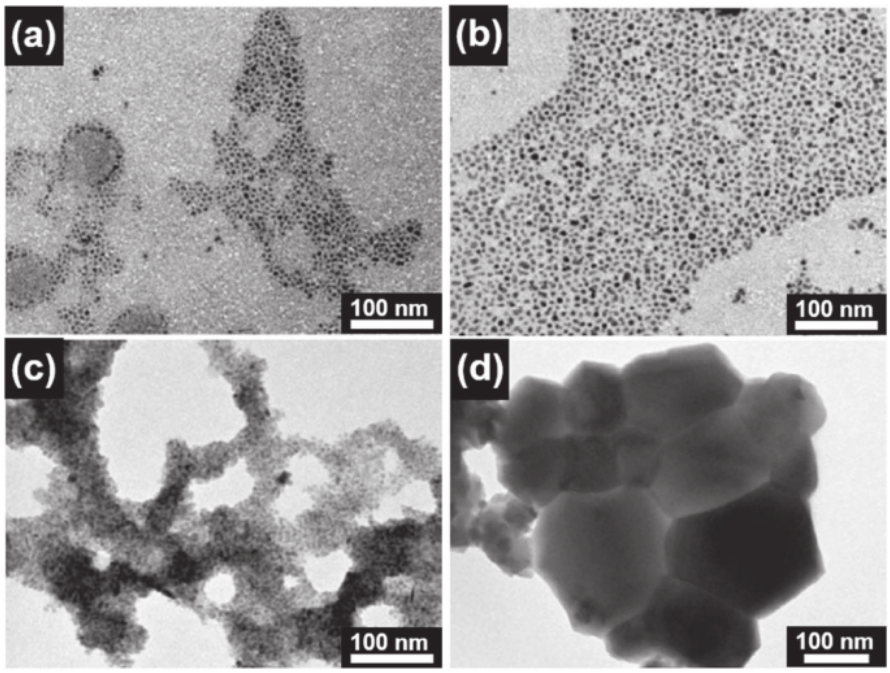

Figure 3. (a) Morphology of as-prepared Fe_3O_4 Morphology of Fe_3O_4 particles produced by thermal decomposition method with the temperature annealing of (b) 300 °C, (c) 700 °C, and (d) 900 °C. Reprinted from publication[44] with permission from Elsevier.

case, PEG-200 and sucrose act as a soft template and capping agent, respectively. The cavity interior of the particle was formed due to the combustion of urea that generates CO_2 bubbles.

Synthesis of Fe_3O_4 through the templating method.—As a sensitive layer for the gas sensor, morphology is one of the critical parameters determining its performance due to its relation to the surface area. As we know, magnetite nanomaterials tend to agglomerate because of their magnetic properties. The templating method can be an excellent strategy to control magnetite's morphology, surface area, pore, and particle size.[58,59] The morphology of materials is controlled during the nucleation and growth stage of the particle formation. This strategy can be divided into hard and soft templating method depending on the template's properties. As its name, a hard template generally is a rigid material that sacrifices its structure to grow the desired material with the same structure as the template.[59] In this approach, three steps should typically be done: template preparation, synthesis material with the template, and template removal. In the case of Fe_3O_4 preparation, several studies report the utilization of a hard template. For instance, Haibo's group used the SiO_2 template or KIT-6 as a sacrificial template.[60] In the first step, KIT-6 was prepared by combining the P123 and TEOS in deionized water containing HCl and n-butanol at 35 °C. The KIT-6 solid product was obtained after the solution was treated hydrothermally at a specific temperature for 24 h and the precipitated was calcined at the temperature of 550 °C for 6 h.

The magnetite with the KIT-6 replica structure was prepared by nano casting technique where the KIT-6 was added to the iron solution and aged 40 °C. After the calcination process in the reduction atmosphere, the template was removed by NaOH leaching. Figure 5 shows the TEM images of the template and Fe_3O_4 particles with the structure of KIT-6. The ordered mesoporous Fe_3O_4 is completely replicate the KIT-6 structure. A similar approach was carried out earlier by Zhu et al.[61] The differences between the two works are the chosen temperature for calcination and reduction process. The calcined and reduction temperatures in Huang's work are 550 °C and 450 °C, respectively, while in Zhu's work, the chosen temperatures are 600 °C and 350 °C. Both works proved that the magnetites have structures similar to KIT-6; however, Huang et al.'s magnetite particles have a surface area of 980 $m^2\ g^{-1}$, about six times higher than the magnetite by Zhu et al.

In their work, Qin et al. used commercial graphene oxide as a template.[62] The sheet of graphene oxide contain abundant sites for the magnetite nucleation. A simple approach was conducted in the preparation, where the iron salt was combined with the graphene oxide sheets solution in the mixture of ethanol and water. The mixture was then stirred at the temperature of ~94 °C until the solvent was evaporated entirely. In this stage, the red powder was obtained, indicating the formation of hematite of Fe_2O_3. The sheet removal was carried out by heating the powder at the temperature of 500 °C. The resulted Fe_2O_3 has a rod-like shape with the length and diameter sizes of 100 nm and 10 nm, respectively. The rods were observed to attach to the graphene oxide sheets. Interestingly, after reduction by the mixture of Ar (95 vol%) and H_2 (5 vol%) gases at 400 °C, the Fe_2O_3 was transformed to the Fe_3O_4, followed by the shape transformation from rod-like to cubic like with the size in the range of 80–120 nm.

Different from hard templating, soft templating does not have a rigid structure. The template, also known as a surfactant, can interact with the iron precursor and control the morphology during crystal growth.[59,63] Several surfactant such as sodium dodecyl sulphonate (SDS),[64] poly(acrylic acid),[65] polyethylene glycol (PEG),[66] etc. Each surfactant will result in a different morphology of the Fe_3O_4. Nanolamelar structure of Fe_3O_4 was obtained by utilizing SDS as a soft template.[64] The iron precursor was mixed with the surfactant and NaOH in the medium of ethanol under a nitrogen atmosphere. The mixing process was conducted at 70 °C to complete the dissolving, and the solution was subjected to reflux treatment at

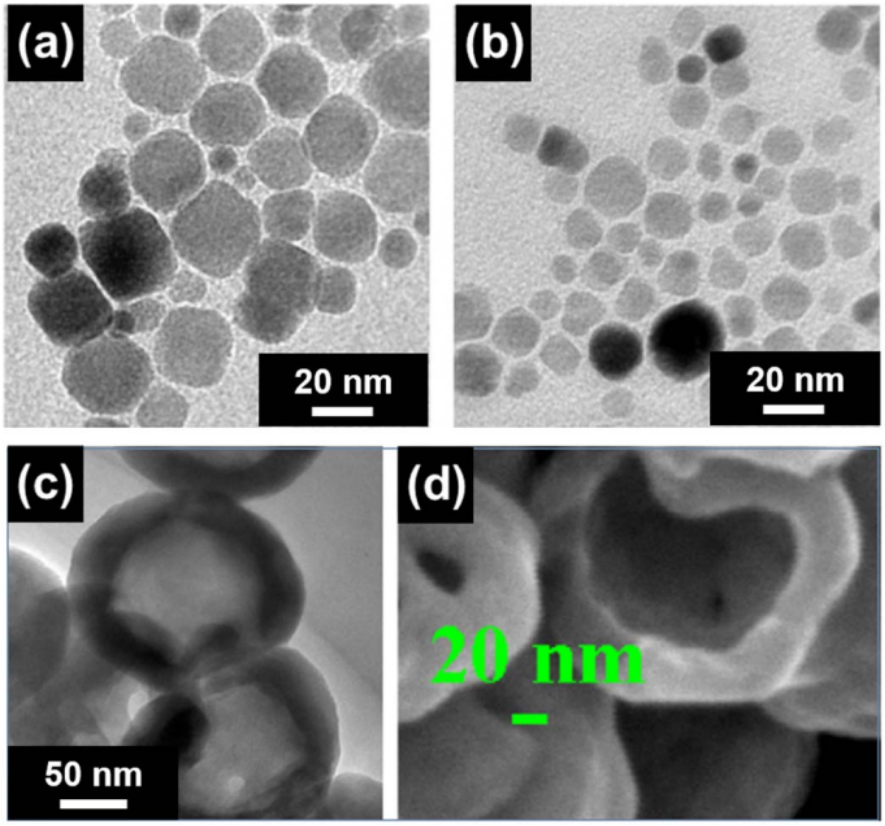

Figure 4. Nanoparticles of Fe_3O_4 synthesized by sol-gel method with the $Fe(AcAc)_3$:HD ratio of 0.11 (a) and 0.22 (b). Reprinted from publication[52] with permission from Elsevier. A hollow sphere of Fe_3O_4 synthesized by PEG-200 assisted hydrothermally (c), (d), Reprinted from publication[57] with permission from Elsevier.

85 °C for 14 h. The nucleation of Fe_3O_4 was occurred on the hydrophilic side of SDS or sulfonic groups, while the hydrophobic side or dodecyl group arranged in back to back manner result in a layered structure. In another work, Fe_3O_4 microsphere was prepared using poly(acrylic acid) by solvothermal method. The process was carried out for two temperature stages, 120 °C for 2 h in the first stage and 200 °C for 10 h in the second stage under a nitrogen atmosphere.[65] This strategy results in a uniform sphere with the size of ∼500 nm.

Furthermore, the oxalic acid was also employed in the post-treatment to etch the contaminant and result in a porous structure. Nanowire morphology was obtained by employing PEG as a template.[66] In their work, Zhang et al. prepared two aqueous solutions where each solution contained sodium hydroxide and the mixture of iron sulfate and PEG-400, respectively. The later solution was added to the first solution dropwise at 80 °C. To get Fe^{3+} state or $Fe(OH)_3$, $NaNO_3$ was added to the mixture solution. This route resulted in a nanowire with a diameter in the range of 5–80 nm and a length up to several micrometers. In this case, PEG-400 is absorbed on the preferred facet of Fe_3O_4 and support anisotropy crystal growth.

Synthesis of Fe_3O_4 through the molten salt method.—The molten salt method is one of the simple strategies to produce metal oxides without solvent employment. This method offers the low-temperature synthesis of material with good crystallization, good morphology, high phase purity, and less defect.[67,68] Generally, one or several salts with low melting temperature points are used, and the reactants have high solubility in the molten salt. The usage of several salts has a proposal to lower the melting temperature. At a specific condition, the precipitate product is then formed after saturation is achieved. There are only a few works that reported the preparation of Fe_3O_4 using this method. For example, a combination of NaCl and KCl salts with the ratio of 1:1 was used as a medium for the formation of octahedral Fe_3O_4 with ferric acetate as an iron source.[64] In the typical procedure, the salts and the ferric acetate were ground to achieve a homogeneous distribution. The final mixture was calcined at various temperatures of 700 °C, 800 °C, and 900 °C. The formation of the octahedral shape of Fe_3O_4 with a uniform size of 1–2 μm was obtained when the calcined temperature is 800 °C, as seen in Fig. 6. In this case, the salts also have a role as a stabilizing agent to decrease the specific facet's surface energy. Iron oleate and sodium sulfate have been used as an iron oxide precursor and salt, respectively, in another report.[69] In their preparation process, both compounds with the ratio of 1:15 was ground and heat to 600 °C for 3 h with the heating rate of 10 °C under Ar atmosphere. The nanocubes of Fe_3O_4 embedded in carbon support with an average size of 20 nm were observed in the TEM and FESEM characterization.

Fe_3O_4 as Sensitive Material for Gas Sensors

Fe_3O_4-based gas sensors.—Compared with other metal oxides, magnetite Fe_3O_4 has unique properties as a half-metallic, where it can be metal or semiconductor depend on its spin direction.[70–74] This property is believed can result in rapid and high sensitivity in gas detection.[72] Therefore, a gas sensor based on the magneto resistor technique can be an alternative strategy to achieve a

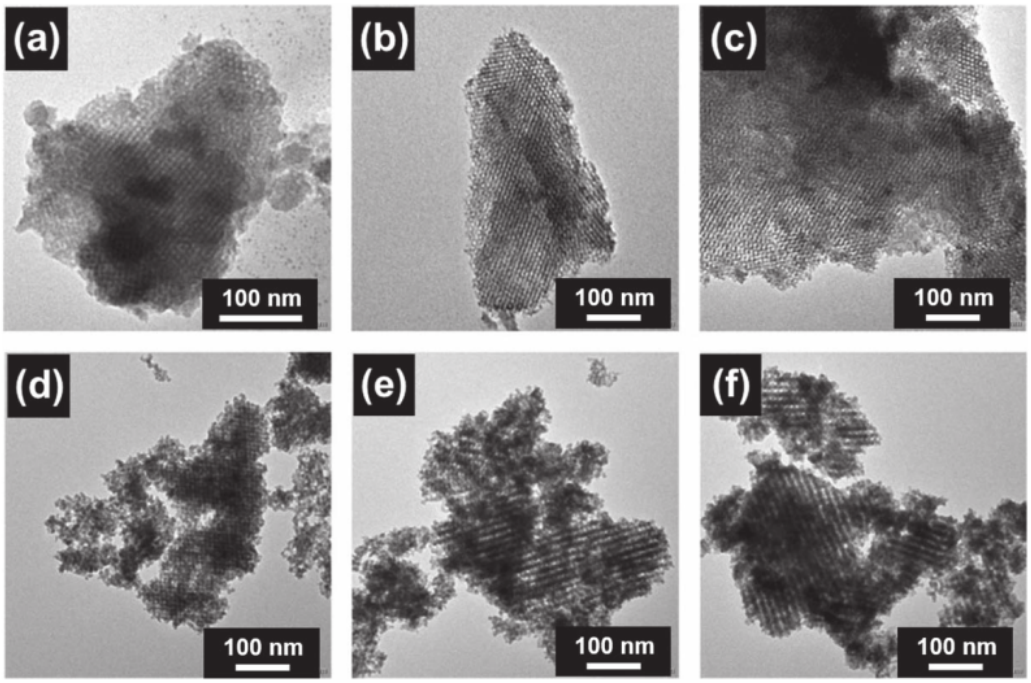

Figure 5. Template of KIT-6 with different aging temperatures of 40 °C (a), 80 °C (b), and 120 °C, respectively, along with the related ordered mesoporous Fe_3O_4, replicate the KIT-6 structure (c)–(e). Reprinted from publication[60] with permission from Elsevier.

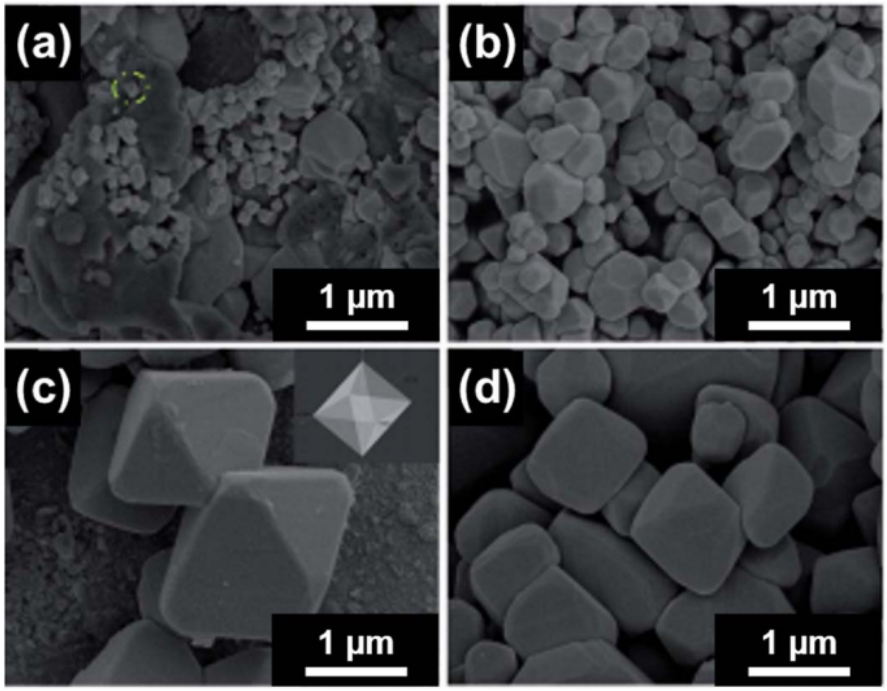

Figure 6. The particles of Fe_3O_4 synthesized by direct calcination of ferric acetate at 700 °C (a). The particles of Fe_3O_4 synthesized by the molten salt method with calcination temperatures of 700 °C (b), 800 °C (c), and 900 °C (d). Reproduced from Ref. 68 with permission from the Royal Society of Chemistry.

high-performance gas sensor. Daniel et al. demonstrated this technique to detect NO gas down to 1.69 ppb.[72] The Fe_3O_4 microspheres with a size of 430 nm were prepared using a hydrothermal method. The presence of NO on the microsphere's surface changes the oxidation state from $Fe^{2+}(d^6)$ to Fe^{3+} (d^5) along with the transformation of spin moments s = 2 to s = 5/2. This transformation changes its conductivity and delivers it as a sensor signal. Their work reported the sensitivity of 14.43% to 500 ppb of NO with a response time of 10–20 s. N-type chemiresistive behavior of Fe_3O_4 was observed by Bertocci et al.[75] The prepared Fe_3O_4 nanoparticles or nanograin with the average size of 16.3 nm success to detect CO and NO_2 at optimal operating temperatures of 260 °C and 220 °C respectively. As a half metal, the magnetite's conductivity is mainly contributed by minority spin channels where hopping electrons from Fe^{2+} to Fe^{3+} occurred and act as electron donors to oxygen ion sorption. Another chemiresistive based on magnetite materials was reported by Ai et al. and Cao et al.[76,77] Fe_3O_4 nanorose and sphere-like particles were prepared to detect ethanol vapor. Two different morphologies were found can deliver different responses. The nanorose exhibited a response of ∼4.4 at room temperature and comparable with the sphere-like that exhibited a response of <10 at 300 °C toward 100 ppm of ethanol. The difference of performances might be contributed by the difference of surface area where the specific surface areas of nanorose and sphere-like Fe_3O_4 are 77 m^2 g^{-1} and 18.6 m^2 g^{-1}, respectively. As seen in Fig. 7, the nanorose was arranged by particles in nanoscale that cause its high specific surface area. It is already well accepted that morphologies directly affect the surface area that determines sensing performance.[3,78,79] However, both reports did not intensely discuss the magnetic factor that might involve in the sensing mechanism.

Metal doped Fe_3O_4 based gas sensors.—Pure Fe_3O_4 based gas sensors typically suffer from the low response and low selectivity. One strategy to improve the gas sensor performance is to add noble metal to the magnetite's surface. The noble metal acts as a catalyst that can convert unreactive analyte to its reactive form leading to an increase in the surface reaction rate, and as a consequence, the sensitivity will increase, and operating temperature will shift to a lower number.[80–83] The increasing response or sensitivity is well believed caused by the increasing number of oxygen ion species on the material surface; the noble metal surface activates the O_2 gas by dissociating it to O species and accelerating the chemisorption process. The vast number of adsorbed oxygen ions associated with a considerable number of active sites provide for the surface reaction. Aside from chemical sensitization, electronic sensitization can be induced by forming Schottky barriers at the interface of noble metal/Fe_3O_4. The gas presence's barrier height can be changed, leading to a change in the magnetite's conductance. However, all benefits that are caused by noble metal may not be achieved simultaneously. For instance, response improvement without reducing operating temperature and response time was observed by Zhai et al. Pd metal was dispersed on the particle surface of Fe_3O_4 and applied to detect ethanol and acetone.[84] Three and five times responses to ethanol and acetone, respectively, compared to the pure counterpart, were observed after dispersing Pd particles at 300 °C. The improving performances are reported due to the increasing oxygen active sites and the Schottky barrier formation at the Pd/Fe_3O_4 interface. The catalyst properties of Pd induce the widening of Fe_3O_4 due to more electron consumption by the dissociated oxygen species (Fig. 8).

Aside from noble metal that can contribute its catalytic properties in analyte detection, transition metal can also be exploited as a dopant. Hwang et al. decorated magnetite nanowire with Mn metal and used it as a CO gas sensor.[85] Interestingly, Fe_3O_4 nanowire did not respond until the operating temperature reached 200 °C. At the same time, Mn-doped Fe3O4 displayed a relatively good response at room temperature with the response and recovery times of 15 s ad 100 s, respectively. The substitution of Mn ion to the Fe sites increases the Fe^{3+} number leading to an increase in the conductivity by a factor of ∼50. Moreover, the substitution also induces the formation of holes as a consequence of charge balancing. Other works also reported this phenomenon.[86] Therefore, Mn-doped Fe_3O_4 has p-type behavior.

Fe_3O_4 composite based gas sensor.—It has been widely reported that combining two different metal oxides to modify electronic structure via fermi alignment can significantly improve gas sensor performance.[87–91] The sensing behavior of composite is determined by the ratio of the two metal oxides. A small amount of modifier will have the same role as a noble metal, where the metal oxide contributes to dissociation of oxygen gas or analyte gas while sensing behavior follows the host counterpart.[92] Moreover, sensing behavior typically follows the primary or significant metal oxide.[80] As an n-type semiconductor, Fe_3O_4 can be combined with a p-type metal oxide to get p-n heterojunction or n-type metal oxide to get n-n heterojunction. Tunable built-in potential in the presence of analyte is believed as a reason for sensor sensitization.

Qu et al. reported the preparation of Fe_3O_4@Co_3O_4 core–shell microspheres through the hydrothermal method as an acetone sensor.[55] Co_3O_4 and Fe_3O_4 themselves show the best performance at operating temperatures of 140 °C and 240 °C, respectively. The oxides' synergy effect causes the core-shell to display its best performance at an operating temperature of 160 °C, where the response value is 102.6 to 100 ppm of acetone. The synergy effect is contributed by the Co_3O_4 shell that is believed to have a thickness close to its debye length (λ_D). Debye length itself is known as the thickness of the layer in which electrons exchange from bulk to surface state.[93] Therefore, the sensitive material's size is pursued close to the length so that the electrons can be fully depleted by the adsorbed oxygens leading to maximizing sensor performance.[93–95] Moreover, the catalytic properties of Co_3O_4 cause an abundance of oxygen ion that, along with the oxygen on the magnetite core, will cause the modulation of sensing performance. Another core-shell system of F_3O_4@NiO was prepared by the same group and applied as a toluene sensor.[96] core-shell with the size of 700 nm displays the response of ∼14 to 100 ppm of toluene at an optimal temperature of 280 °C. However, the sensor might have low selectivity, especially against xylene, because the response value to toluene is only double that of xylene.

Beautiful three-dimensional inverse opal (3DIO) ZnO-Fe_3O_4 has been prepared by Zhang et al. for acetone sensor.[119] Macropores structure was observed due to the template structure's replica (PMMA), see Fig. 9. It was found that the mesoporous structure in the skeleton was increased as the Fe_3O_4 concentration increased to 20%. The combination of macropores and mesopores structures increases the number of active sites significantly. As a consequence, the gas sensor performances increase. They also claimed that the magnetite acts as a surface-depletion controlled type of sensor material that also contributes to the sensor improvement. The composite shows its best performance at 485 °C with the response of 47 to 50 ppm of acetone. In this case, the magnetite is present as a supporting material of the ZnO.

Aside from metal oxide-Fe_3O_4, the composite based on magnetite material can be built by the combination of Fe_3O_4 and carbon nanomaterials such as Reduced Graphene Oxide (rGO) and Multiwalled Carbon Nanotubes (MWCNT). It is well known that both carbons have *p-type* semiconductor characteristic and its arrangement with n-type material such as F_3O_4 will generate a tunable space charge region in the heterojunction which contribute in the enhancement of gas sensor performance.[5,97–101] For instance, the Fe_3O_4, which has a work function of 5.2 eV, was contacted with rGO, which has a work function of 6.8 eV in core@shell formation.[102] Due to its difference, Fermi alignment occurred as the electrons in the Fe_3O_4 conduction band transferred to the rGO result in a space charge region associated with built-in potential. The change in the potential during NO_2 exposure is believed to be one reason for the high response of the core@shell to NO_2 at room temperature. The heterojunction phenomenon is also observed in Fe_3O_4-MWCNT-PhCOOH based ammonia sensor.[103] Aside from the phenyl group with a particular interaction with ammonia, the change in barrier height during ammonia detection results in a high electrical resistance chance. In their case, the composite displays a

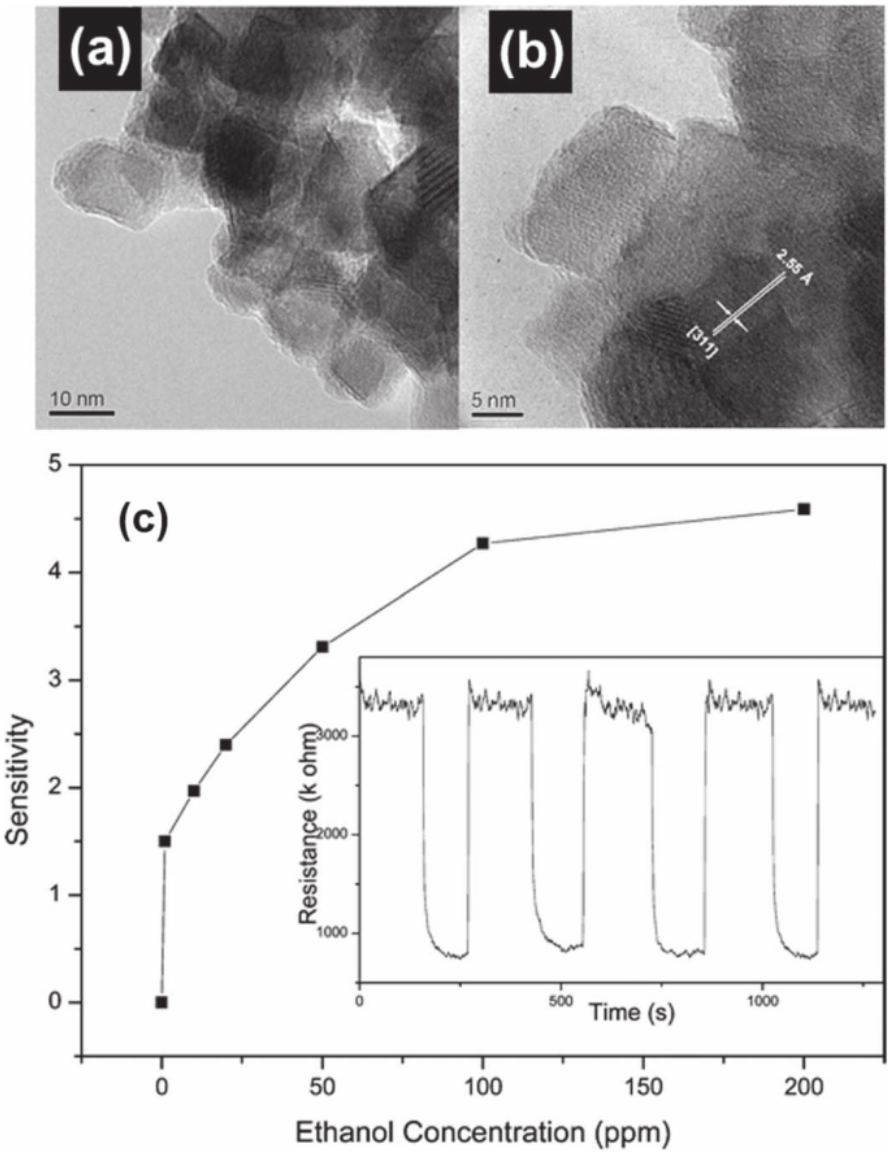

Figure 7. TEM image of Fe_3O_4 nanoparticles that arranged the nanorose structure (a), (b) and its performances as ethanol sensor (c). Reprinted from publication[76] with permission from copyright 2010 American Chemical Society.

relatively high response to 4000 ppm of ammonia at 50 °C compare to MWCNT and MWCNT-COOH, indicating both the phenyl group and Fe_3O_4 give a vital role in ammonia detection.

Sensing mechanism of Fe_3O_4 and its modification.—In general, metal oxide gas sensors, including Fe_3O_4, have both receptor and transducer functions. As a receptor, the oxide surface facilitates the reaction between oxygen ion species and the gas, while as a transducer, the oxide will deliver the change of electrical properties due to the surface reaction as a signal.[78,104–106] In the receptor function, the sensing mechanism highly depends on the oxygen species number on the oxide surface. At a specific temperature, the oxygens from the air will be adsorbed, dissociated, and ionized by extracting electrons from oxide surfaces leading to a change in the resistance of metal oxides. In Fe_3O_4, its n-type behavior causes the resistance to increase when the ion sorption occurs. The kind of oxygen species on the surfaces is highly dependent on temperature due to its creation is categorized as an activated reaction.[3,5,107,108] At below 100 °C, O_2^- will be created (Eq. 2); at 100 °C–300 °C and above 300 °C, the species of O_2^- will be reduced to O^- (Eq. 3) and O^{2-} (Eq. 4), respectively.

$$O_2(gas) \Leftrightarrow O_2(ads) \quad [1]$$

$$O_2(ads) + e^- \Leftrightarrow O_2^-(ads) \quad [2]$$

$$O_2^-(ads) + e^- \Leftrightarrow 2O^-(ads) \quad [3]$$

$$O^- + e^- \Leftrightarrow O^{2-}(ads) \quad [4]$$

In the electron trapping process by the adsorbed oxygen, the electron depletion layer is generated, and the change of width layer

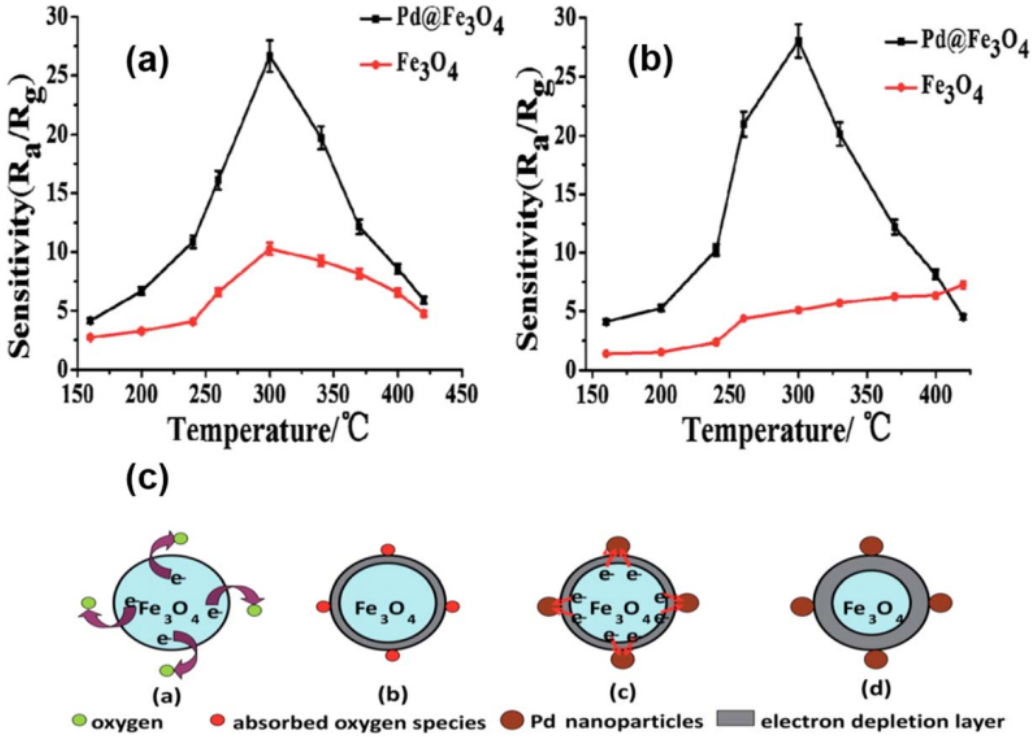

Figure 8. Sensing performance of Pd doped Fe_3O_4 to 100 ppm ethanol (a) and 100 ppm acetone (b) at different temperatures. The effect of Pd nanoparticles on the surface of Fe_3O_4 (c). Reproduced from Ref. 84 with permission from the Royal Society of Chemistry.

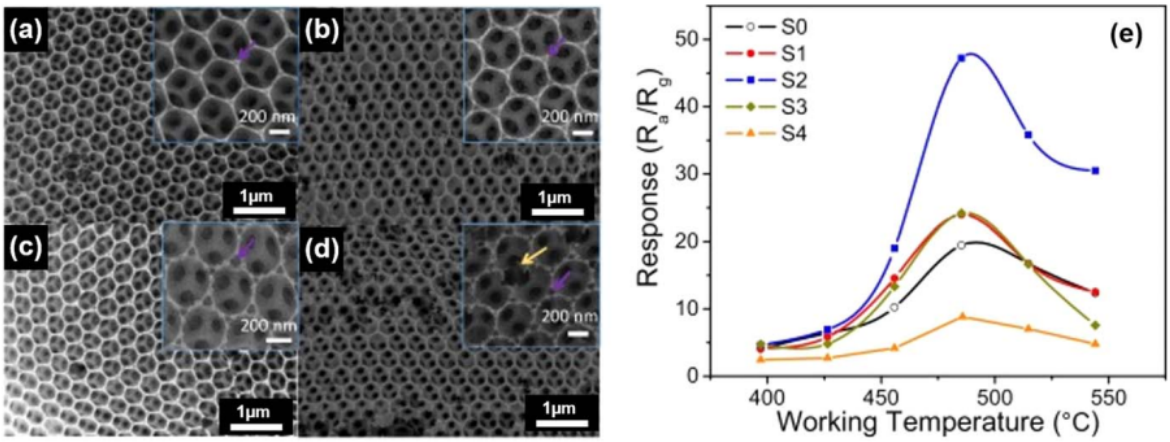

Figure 9. Morphologies of pure ZnO (a), ZnO:Fe_3O_4 with ratio of 1:10 (b), 2:10 (c), and 3:10 (d). Sensing performance comparison of pure ZnO (S0), ZnO:Fe_3O_4 with a ratio of 1:10 (S1), 2:10 (S2), 3:10 (S3), and ZnO without template (S4) (e). Reprinted from publication[119] with permission from Elsevier.

is delivered by the transducer function. The width layer that is associated with the Schottky barrier determines the sensor performance, especially if it is related to the particle size. As in *D-L* theory, when D (particle diameter) $\gg 2L$ (width layer), the sensing performances are determined by the change of the double Schottky barriers at magnetite grain boundaries.[78,109,110] When $D = 2L$, the performances are determined by the necks between grains, and finally, when $D \ll 2L$, the performances are determined by each particle or grain. Therefore, the development of magnetite-based sensors nowadays is focused on size control or morphological control.

During gas exposure, the width layer can be narrowing or widening, depending on the type of gas. Surface interaction with reducing gas such as CO, CO_2, and SO_2 will cause the layer's narrowing and reduce resistance as a result. The example of the responsible surface reaction between reduction gas and oxygen ions can be seen in Eq. 5.[111,112] On the other hand, surface interaction with an oxidizing gas such as NO and NO_2 will cause layer widening

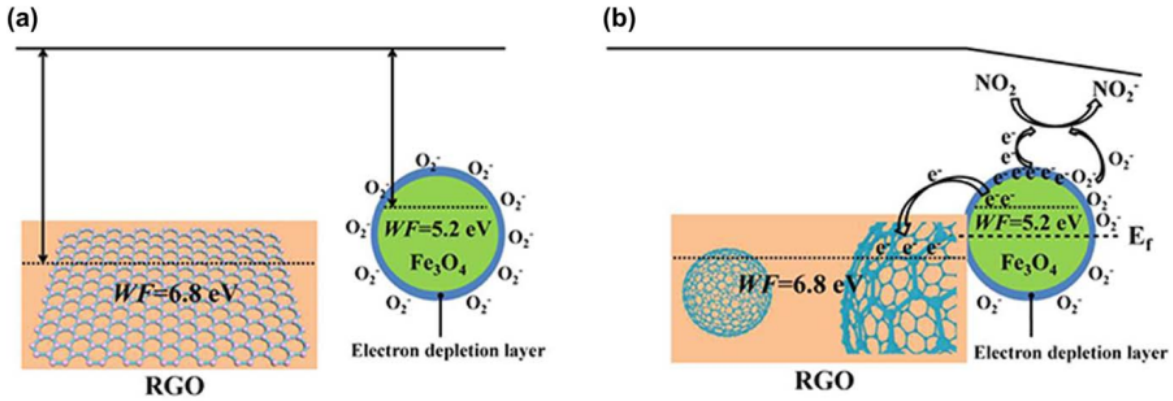

Figure 10. Illustration of sensing mechanism of the p-n junction of RGO-Fe_3O_4 before (a) and during (b) fermi alignment. Reprinted from publication[102] with permission from Frontiers.

and increase resistance. The example of the responsible surface reaction can be seen in Eqs. 6 and 7.[102,113,114]

$$CO(ads) + O^-(ads) \Leftrightarrow CO_2(ads) + e^- \quad [5]$$

$$NO_2(ads) + e^-(ads) \Leftrightarrow NO_2{}^-(ads) \quad [6]$$

$$NO_2(ads) + O^-(ads) \Leftrightarrow NO^- + O_2(gas) \quad [7]$$

Incorporating other constituents such as doping or composite can improve the magnetite sensing performances by contributing to the mechanism. Metal doping contributes to chemical and electronic sensitization.[84,115–117] The transformation of unreactive gas to reactive gas by spillover phenomenon on the metal surface can improve sensitivity and selectivity and increase the rate reaction leading to reduce its response time.[80] Moreover, the additional Schottky barrier located on the metal/Fe_3O_4 interface as generated by the difference between metal work function and Fe_3O_4 electron affinity can improve the transducer function leading to improve sensing performances.[80] As proposed by Zhai et al.[84], the presence of noble metal nanoparticles on the surface of Fe_3O_4 catalyzes the oxygen molecule's dissociation to increase electron consumption by the oxygen itself. Under ambient atmosphere, similar to the pure Fe_3O_4, oxygen molecules are adsorbed, dissociated, and ionized by taking electrons from the oxide's surface; with a noble metal such as Pd, the dissociation becomes faster, leading to more oxygen species on the magnetite surface. With the more electrons that are consumed by the oxygen, the depletion layer becomes wider. As a consequence, its change due to gas-surface interaction becomes higher.

The presence of the second phase (X) in the Fe_3O_4 system will cause the heterojunction to occur on both interfaces. This heterojunction is reported to contribute to the additional barrier that causes a more considerable change in their resistance during the detection. Moreover, the second phase's defect can also increase the number of oxygen species on the surface. As stated earlier, Fe_3O_4 can be combined with p-type semiconductor such as rGO forming p–n heterojunction, and with n-type such as ZnO forming n-n heterojunction. The gas sensor improvement is achieved due to the addition of the depletion layer located on the interface of X/Fe_3O_4. Since there are differences between the two energy levels, electron transfer and fermi alignment occur along with the depletion layer's generation.[87,118] The depletion layer's width is sensitive to gas, hence contributing to the gas sensor performances. An example of an illustration of the sensing mechanism can be seen in Fig. 10.

As a part of magnetic materials, the sensing mechanism can be contributed by the change in magnetite properties such as magnetization saturation and coercivity that induce the change in conductivity.[72] The reducing or oxidizing Fe ion in the Fe_3O_4 by gas interaction changes its spin state, leading to a change in the conductivity. The change of conductivity is then delivered as a sensor signal.

Table I. Summary of gas sensors based on Fe_3O_4 nanomaterials.

Materials	Gas and concentration	T*sens* (°C)	Response	References
Fe_3O_4 microsphere	NO, 500 ppb	RT	14.43%	72
Fe_3O_4 nanoparticles	CO, 1000 ppm	260	55%	75
Fe_3O_4 nanoparticles	NO_2, 12 ppm	220	180%	75
Fe_3O_4 nanorose	Ethanol, 100 ppm	RT	~4.4	76
Fe_3O_4 sphere	Ethanol, 100 ppm	300	<10	77
Fe_3O_4 nanoparticles	Ethanol, 100 ppm	300	~10	84
Fe_3O_4 nanoparticles	Acetone, 100 ppm	300	~5	84
Pd-doped Fe_3O_4	Ethanol, 100 ppm	300	~28	84
Pd-doped Fe_3O_4	Acetone, 100 ppm	300	~28	84
Pd-doped Fe_3O_4 halloysite nanotubes	H_2, 100 ppm	400	19.8	117
Fe_3O_4-HNTs-APTES-Palladium (M-HNTs-A-Pd) nanocomposite	H_2, 50 ppm	300	80.1	120
Fe_3O_4/MWCNT-PhCOOH	NH_3, 2000 ppm	50	~2	103
Cu_2O@Fe_3O_4	Ethanol, 360 ppm	250	10.84	121
Fe_3O_4/C nanoflakes	Ethyl acetate, 100 ppm	370	~7	69
Fe_3O_4@Co_3O_4 core–shell microspheres	Acetone, 100 ppm	160	102.6	55
F_3O_4@NiO core–shell	Toluene, 100 ppm	280	~14	96
three-dimensional inverse opal (3DIO)/ZnO-Fe_3O_4	Acetone, 50 ppm	485	47	119

Future Perspective

Based on the performance summary of gas sensors based on Fe_3O_4 in Table I, the development of Fe_3O_4 as a gas sensor material in the future still has a very high prospect. Fe_3O_4 can be developed as a gas sensor in two aspects: a metal oxide gas sensor and a magnonic sensor. As a typical metal oxide sensor, its surface is sensitive to the presence of gas; however, selectivity is also an obstacle for its development as a gas sensor. Moreover, due to the change in magnetic properties unique for each type of gas, selectivity should not be a problem as a magnonic sensor. The combination of the high sensitivity of the metal oxide sensor and the high selectivity of the magnonic sensor possessed by Fe_3O_4 is believed to produce a superior gas sensor in the future. Improving Fe_3O_4-based gas sensors' performance can also be focused on optimizing the synergy effect of Fe_3O_4 and other metal oxides or carbon nanomaterials in composite form. The low bandgap of Fe_3O_4 compared to other metal oxides can generate heterojunctions that contribute to the detection mechanism. That property can be utilized in forming p–n junctions and n-n junctions. To maximize the resulting junction, one should pay attention to the second phase dispersion or connection with Fe_3O_4 particles, which, of course, can be achieved by optimizing the synthesis method used. Other nanoparticles are still very wide opened in composites with Fe_3O_4 as a gas sensor material such as ZnO, SnO_2, and others. Furthermore, a combination of metal dispersion over Fe_3O_4 particles and connection of Fe_3O_4 with metal oxides or other carbon nanomaterials can be made to maximize receptor and transducer functions. This has the potential to produce a gas sensor with high sensitivity and selectivity.

Also, exploration of these materials' morphology is still limited, and the seeking of the unique morphologies that involve the usage of capping agent, complexing agent, or soft template, is still a wide-open challenge. Indeed, the challenge can also be completed by a new strategy or route in their preparation. Several challenges still exist in the preparation, including suppressing grain growth, preventing agglomeration, and determining the architecture of the Fe_3O_4 particles.

Acknowledgments

The authors acknowledge financial grants provided by Lembaga Pengelola Dana Pendidikan (LPDP), Ministry of Finance of Indonesia. This work is also partially supported by the Indonesia Ministry of Education and Culture, and the Indonesia Ministry of Research and Technology under the World Class University Program's grant scheme managed by Institut Teknologi Bandung.

ORCID

Mochammad Zakki Fahmi https://orcid.org/0000-0001-5430-9992
Syahrul Humaidi https://orcid.org/0000-0003-2183-3282
Brian Yuliarto https://orcid.org/0000-0003-0662-7923

References

1. S. Chakrabarti and B. K. Dutta, *J. Hazard. Mater.*, **112**, 269 (2004).
2. A. Ramadoss and S. J. Kim, *Mater. Chem. Phys.*, **140**, 405 (2013).
3. N. L. W. Septiani et al., *ACS Appl. Nano Mater.*, **3**, 8982–8996 (2020).
4. N. L. W Septiani and B. Yuliarto, *Appl. Phys. A*, **123**, 166 (2017).
5. N. L. W. Septiani, Y. V. Kaneti, B. Yuliarto, H. K. D Nugraha, T. Takei, J. You, and Y. Yamauchi, *Sensors and Actuators, B: Chemical*, **261**, 241 (2018).
6. R. K. Selvan, I. Perelshtein, N. Perkas, and A. Gedanken, *The Journal of Physical Chemistry C*, **112**, 1825 (2008).
7. C. Kim, M. Noh, M. Choi, J. Cho, and B. Park, *Chem. Mater.*, **17**, 3297 (2005).
8. D. Mei, X. Yuan, Z. Ma, P. Wei, X. Yu, J. Yang, and Z.-F. Ma, *ACS Applied Materials & Interfaces*, **8**, 12804 (2016).
9. S. Tanaka, Y. V. Kaneti, N. L. W. Septiani, S. X. Dou, Y. Bando, M. S. A. Hossain, J. Kim, and Y. Yamauchi, *Small Methods*, **3**, 1800512 (2019).
10. L. M. Pastrana-Martínez, N. Pereira, R. Lima, J. L. Faria, H. T. Gomes, and A. M. T. Silva, *Chem. Eng. J.*, **261**, 45 (2015).
11. D. Han and M. Zhao, *J. Alloys Compd.*, **815**, 152406 (2020).
12. K. A. Owusu et al., *Nat. Commun.*, **8**, 14264 (2017).
13. Z. Liu, S. W. Tay, and X. Li, *Chem. Commun.*, **47**, 12473 (2011).
14. R. Rahmawati, Y. V. Kaneti, A. T. Sunaryono, B. Y. Suyatman, D. K. Nugraha, S. A. Hossain, and Y. Yamauchi, *Bull. Chem. Soc. Jpn.*, **91**, 311 (2018).
15. G. V. M. Williams, T. Prakash, J. Kennedy, S. V. Chong, and S. Rubanov, *J. Magn. Magn. Mater.*, **460**, 229 (2018).
16. W. Jiang, M. Pelaez, D. D. Dionysiou, M. H. Entezari, D. Tsoutsou, and K. O'Shea, *Chem. Eng. J.*, **222**, 527 (2013).
17. T. Tuutijärvi, J. Lu, M. Sillanpää, and G. Chen, *J. Hazard. Mater.*, **166**, 1415 (2009).
18. X. Huang, Y. Chen, E. Walter, M. Zong, Y. Wang, X. Zhang, O. Qafoku, Z. Wang, and K. M. Rosso, *Environmental Science & Technology*, **53**, 10197 (2019).
19. K. Rajendran and S. Sen, *Environmental Nanotechnology, Monitoring & Management*, **9**, 122 (2018).
20. G. Shi, B. Sun, Z. Jin, J. Liu, and M. Li, *Sensors Actuators B*, **171–172**, 699 (2012).
21. D. Zhang, Z. Liu, S. Han, C. Li, B. Lei, M. P. Stewart, J. M. Tour, and C. Zhou, *Nano Lett.*, **4**, 2151 (2004).
22. S. M. Taimoory, A. Rahdar, M. Aliahmad, F. Sadeghfar, M. R. Hajinezhad, M. Jahantigh, P. Shahbazi, and J. F. Trant, *J. Mol. Liq.*, **265**, 96 (2018).
23. A. Dash, M. T. Ahmed, and R. Selvaraj, *J. Mol. Struct.*, **1178**, 268 (2019).
24. L. M. Sanchez and V. A. Alvarez, *Bioengineering.*, **6**(3), 1 (2019).
25. T. Marín, P. Montoya, O. Arnache, R. Pinal, and J. Calderón, *Mater. Des.*, **152**, 78 (2018).
26. T. T. Tung, N. V. Chien, N. Van Duy, N. Van Hieu, M. J. Nine, C. J. Coghlan, D. N. H. Tran, and D. Losic, *J. Colloid Interface Sci.*, **539**, 315 (2019).
27. T. Parandhaman, N. Pentela, B. Ramalingam, D. Samanta, and S. K. Das, *ACS Sustainable Chemistry & Engineering*, **5**, 489 (2017).
28. B. Ramalingam, T. Parandhaman, P. Choudhary, and S. K. Das, *ACS Sustainable Chemistry & Engineering*, **6**, 6328 (2018).
29. J. Kim et al., *ACS Applied Materials & Interfaces*, **10**, 41935 (2018).
30. J. Blasco, J. Garcia, and G. Subias, "Structural transformation in magnetite below the Verwey transition." *Physical Review B*, **84**, 104105 (2011).
31. A. S. Teja and P.-Y. Koh, *Prog. Cryst. Growth Charact. Mater.*, **55**, 22 (2009).
32. A. Kale, S. Gubbala, and R. D. K. Misra, *J. Magn. Magn. Mater.*, **277**, 350 (2004).
33. N. A. Spaldin, *Magnetic Materials: Fundamentals and Applications* (Cambridge University Press, Cambridge) 2nd ed. (2010).
34. J. Gao, H. Gu, and B. Xu, *Acc. Chem. Res.*, **42**, 1097 (2009).
35. J. Noh, O. I. Osman, S. G. Aziz, P. Winget, and J.-L. Brédas, *Sci. Technol. Adv. Mater.*, **15**, 44202 (2014).
36. S. Impeng, A. Junkaew, P. Maitarad, N. Kungwan, D. Zhang, L. Shi, and S. Namuangruk, *Appl. Surf. Sci.*, **473**, 820 (2019).
37. D. Matatagui, O. V. Kolokoltsev, N. Qureshi, E. V. Mejía-Uriarte, C. L. Ordoñez-Romero, A. Vázquez-Olmos, and J. M. Saniger, *Sensors Actuators B*, **240**, 497 (2017).
38. Y. Yong, X. Su, Q. Zhou, Y. Kuang, and X. Li, *Sci. Rep.*, **7**, 17505 (2017).
39. E. R. Kumar, R. Jayaprakash, G. S. Devi, and P. Siva Prasada Reddy, *Sensors Actuators B*, **191**, 186 (2014).
40. T. Q. Bui, S. N.-C. Ton, A. T. Duong, and H. T. Tran, *Journal of Science: Advanced Materials and Devices*, **3**, 107 (2018).
41. S. E. Favela-Camacho, J. F. Pérez-Robles, P. E. García-Casillas, and A. Godinez-Garcia, *J. Nanopart. Res.*, **18**, 176 (2016).
42. C. Cao, L. Xiao, C. Chen, X. Shi, Q. Cao, and L. Gao, *Powder Technol.*, **260**, 90 (2014).
43. E. Darezereshki, A. K. Darban, M. Abdollahy, and A. Jamshidi, *J. Alloys Compd.*, **749**, 336 (2018).
44. D. Amara, I. Felner, I. Nowik, and S. Margel, *Colloids Surf., A*, **339**, 106 (2009).
45. V. Patsula et al., *ACS Applied Materials & Interfaces*, **8**, 7238 (2016).
46. Z. Xu, C. Shen, Y. Hou, H. Gao, and S. Sun, *Chem. Mater.*, **21**, 1778 (2009).
47. W. Glasgow, B. Fellows, B. Qi, T. Darroudi, C. Kitchens, L. Ye, T. M. Crawford, and O. T. Mefford, *Particuology*, **26**, 47 (2016).
48. I. A. Neacşu, A. I. Nicoară, O. R. Vasile, and B. Ş. Vasile, *Nanobiomaterials in Hard Tissue Engineering*, ed. M. G Alexandru (William Andrew Publishing, Norwich, NY) p. 271 (2016).
49. E. Yilmaz and M. Soylak, *Handbook of Nanomaterials in Analytical Chemistry*, ed. C. M. Hussain (Elsevier, Amsterdam) p. 375 (2020).
50. P. Hu, T. Chang, W.-J. Chen, J. Deng, S.-L. Li, Y.-G. Zuo, L. Kang, F. Yang, M. Hostetter, and A. A. Volinsky, *J. Alloys Compd.*, **773**, 605 (2019).
51. H. Cui, Y. Liu, and W. Ren, *Adv. Powder Technol.*, **24**, 93 (2013).
52. C. Sciancalepore, A. F. Gualtieri, P. Scardi, A. Flor, P. Allia, P. Tiberto, G. Barrera, M. Messori, and F. Bondioli, *Mater. Chem. Phys.*, **207**, 337 (2018).
53. E. B. Denkbaş, E. Çelik, E. Erdal, D. Kavaz, Ö. Akbal, G. Kara, and C. Bayram, *Nanobiomaterials in Drug Delivery*, ed. A. M. B. T.-N. and D. D. Grumezescu (William Andrew Publishing, Norwich, NY) 9, 285 (2016).
54. A. D. Li and W. C. Liu, *Woodhead Publishing Series in Composites Science and Engineering*, ed. S. C. Tjong and Y.W Mai (Woodhead Publishing, Cambridge) 108 (2010).
55. F. Qu, J. Liu, Y. Wang, S. Wen, Y. Chen, X. Li, and S. Ruan, *Sensors Actuators B*, **199**, 346 (2014).
56. A. C. B. Jesus, J. R. Jesus, R. J. S. Lima, K. O. Moura, J. M. A. Almeida, J. G. S. Duque, and C. T. Meneses, *Ceram. Int.*, **46**, 11149 (2020).
57. G. Gao, P. Qiu, Q. Qian, N. Zhou, K. Wang, H. Song, H. Fu, and D. Cui, *J. Alloys Compd.*, **574**, 340 (2013).
58. Z. Peng, X. Liu, H. Meng, Z. Li, B. Li, Z. Liu, and S. Liu, *ACS Applied Materials & Interfaces*, **9**, 4577 (2017).

59. Y. Xie, D. Kocaefe, C. Chen, Y. Kocaefe, and S. Seki, Editor.*J. Nanomater.*, **2016**, 2302595 (2016).
60. Y. Huang, Y. Zhang, D. Liu, M. Li, Y. Yu, W. Yang, and H. Li, *Talanta*, **201**, 511 (2019).
61. S. Zhu, B. Dong, Y. Yu, L. Bu, J. Deng, and S. Zhou, *Chem. Eng. J.*, **328**, 527 (2017).
62. Z. Qin, Z.-H. Ma, J.-K. Zhi, and Y.-L. Fu, *Rare Met.*, **38**, 764 (2019).
63. A. F. Sierra-Salazar, A. Ayral, T. Chave, V. Hulea, S. I. Nikitenko, S. Abate, S. Perathoner, and P. Lacroix-Desmazes, *Horizons in Sustainable Industrial Chemistry and Catalysis* (Elsevier, Amsterdam) vol. 178, 377 (2019).
64. J. Wang, J. Xu, X. Meng, and Y. Huang, *Mater. Res. Bull.*, **49**, 176 (2014).
65. Y. Yu, Y. Li, Y. Wang, and B. Zou, *Langmuir*, **34**, 9359 (2018).
66. H. Zhang, J. Zhao, and X. Ou, *Mater. Lett.*, **209**, 48 (2017).
67. X. Wen, C. He, B. Wu, X. Huang, Z. Huang, Z. Yin, Y. Liu, M. Fang, X. Wu, and X. Min, *CrystEngComm*, **21**, 1809 (2019).
68. C. Shang, G. Ji, W. Liu, X. Zhang, H. Lv, and Y. Du, *RSC Adv.*, **5**, 80450 (2015).
69. X. Liang, Y. Qin, W. Xie, Z. Deng, C. Yang, and X. Su, *J. Alloys Compd.*, **818**, 152898 (2020).
70. M. Watanabe and S. Abe, *J. Nanosci. Nanotechnol.*, **16**, 2509.
71. A. D Fauzi, M. A Majidi, and A. Rusydi, *J. Phys. Condens. Matter*, **29**, 135802 (2017).
72. T. T. Daniel, S. Majumder, V. K. S. Yadav, and R. Paily, *IEEE Sensors Journal*, **20**, 13341 (2020).
73. X. Hou, X. Wang, and W. Mi, *J. Alloys Compd.*, **765**, 1127 (2018).
74. M. Kurahashi, X. Sun, and Y. Yamauchi, *Physical Review B*, **81**, 193402 (2010).
75. F. Bertocci, A. Fort, M. Mugnaini, V. Vignoli, E. Bertolucci, M. Marracci, A. M. R. Galletti, and B. Tellini, *2016 IEEE Metrology for Aerospace (MetroAeroSpace)*, p. 286 (2016).
76. Z. Ai, K. Deng, Q. Wan, L. Zhang, and S. Lee, *The Journal of Physical Chemistry C*, **114**, 6237 (2010).
77. Y. Cao, H. Qin, X. Niu, and D. Jia, *Ceram. Int.*, **42**, 10697 (2016).
78. A. Dey, *Materials Science and Engineering B: Solid-State Materials for Advanced Technology*, **229**, 206 (2018).
79. Y. V. Kaneti, N. L. W. Septiani, I. Saptiama, X. Jiang, B. Yuliarto, M. J. A. Shiddiky, N. Fukumitsu, Y.-M. Kang, D. Golberg, and Y. Yamauchi, *Journal of Materials Chemistry A*, **7**, 3415 (2019).
80. D. Degler, U. Weimar, and N. Barsan, *ACS Sens.*, **4**, 2228 (2019).
81. C. Liu, Q. Kuang, Z. Xie, and L. Zheng, *Cryst. Eng. Comm*, **17**, 6308 (2015).
82. Y. V. Kaneti, X. Zhang, M. Liu, D. Yu, Y. Yuan, L. Aldous, and X. Jiang, *Sensors and Actuators, B: Chemical*, **230**, 581 (2016).
83. A. Debataraja, N. L. W. Septiani, B. Yuliarto, B. S Nugraha, and H. Abdullah, *Ionics*, **25**, 4459 (2019).
84. Q. Zhai, B. Du, R. Feng, W. Xu, and Q. Wei, *Anal. Methods*, **6**, 886 (2014).
85. S. O. Hwang, C. H. Kim, Y. Myung, S.-H. Park, J. Park, J. Kim, C.-S. Han, and J.-Y. Kim, *The Journal of Physical Chemistry C*, **112**, 13911 (2008).
86. J. Wu, Q. Huang, D. Zeng, S. Zhang, L. Yang, D. Xia, Z. Xiong, and C. Xie, *Sensors Actuators B*, **198**, 62 (2014).
87. D. R. Miller, S. A. Akbar, and P. A. Morris, *Sensors and Actuators, B: Chemical*, **204**, 250 (2014).
88. M. Poloju, N. Jayababu, E. Manikandan, and M. V. R. Reddy, *Journal of Materials Chemistry C*, **5**, 2662 (2017).
89. Q. Yu, J. Zhu, Z. Xu, and X. Huang, *Sensors Actuators B*, **213**, 27 (2015).
90. L. Wang, Z. Lou, R. Zhang, T. Zhou, J. Deng, and T. Zhang, *ACS Applied Materials & Interfaces*, **8**, 6539 (2016).
91. J. Zhang, L. Zhang, D. Leng, F. Ma, Z. Zhang, Y. Zhang, W. Wang, Q. Liang, J. Gao, and H. Lu, *Sensors Actuators B*, **306**, 127575 (2020).
92. Y. J. Kwon, A. Mirzaei, S. Y. Kang, M. S. Choi, J. H. Bang, S. S. Kim, and H. W. Kim, *Appl. Surf. Sci.*, **413**, 242 (2017).
93. B. Wang, L. F. Zhu, Y. H. Yang, N. S. Xu, and G. W. Yang, *The Journal of Physical Chemistry C*, **112**, 6643 (2008).
94. X. Du and S. M. George, *Sensors Actuators B*, **135**, 152 (2008).
95. K. D. Schierbaum, U. Weimar, W. Göpel, and R. Kowalkowski, *Sensors Actuators B*, **3**, 205 (1991).
96. F. Qu, Y. Wang, J. Liu, S. Wen, Y. Chen, and S. Ruan, *Mater. Lett.*, **132**, 167 (2014).
97. N. L. W Septiani and B. Yuliarto, *Journal of The Electrochemical Society*, **163**, B97 (2016).
98. A. Vass, P. Berki, Z. Nemeth, B. Reti, and K. Hernadi, *physica status solidi (b)*, **250**, 2554 (2013).
99. P. Tyagi, A. Sharma, M. Tomar, and V. Gupta, *Sensors Actuators B*, **248**, 980 (2017).
100. P. Potirak, W. Pecharapa, and W. Techitdheera, *J. Exp. Nanosci.*, **9**, 96 (2014).
101. N. H. Ha, D. D. Thinh, N. T. Huong, N. H. Phuong, P. D. Thach, and H. S. Hong, *Appl. Surf. Sci.*, **434**, 1048 (2018).
102. C. Zou et al., *Frontiers in Materials*, **6**, 195 (2019).
103. A. Pistone, A. Piperno, D. Iannazzo, N. Donato, M. Latino, D. Spadaro, and G. Neri, *Sensors Actuators B*, **186**, 333 (2013).
104. N. Yamazoe and K. Shimanoe, *Sensors Actuators B*, **138**, 100 (2009).
105. N. Yamazoe, K. Shimanoe, and M. Penza, Editor*Journal of Sensors*, **2009**, 875704 (2009).
106. Z. Hua, C. Tian, D. Huang, W. Yuan, C. Zhang, X. Tian, M. Wang, and E. Li, *Sensors Actuators B*, **267**, 510 (2018).
107. Y. Wang, P. Cheng, X. Li, C. Wang, C. Feng, and G. Lu, *Journal of Materials Chemistry C*, **8**, 78 (2020).
108. M. Gardon and J. M. Guilemany, *J. Mater. Sci., Mater. Electron.*, **24**, 1410 (2013).
109. X. Zhou, A. Wang, Y. Wang, L. Bian, Z. Yang, Y. Bian, Y. Gong, X. Wu, N. Han, and Y. Chen, *ACS Sens.*, **3**, 2385 (2018).
110. M. Tonezzer and N. V. Hieu, *Sensors Actuators B*, **163**, 146 (2012).
111. S. Mahajan and S. Jagtap, *Applied Materials Today*, **18**, 100483 (2020).
112. D. Panda, A. Nandi, S. K. Datta, H. Saha, and S. Majumdar, *RSC Adv.*, **6**, 47337 (2016).
113. J. Hu, C. Zou, Y. Su, M. Li, Y. Han, E. S.-W. Kong, Z. Yang, and Y. Zhang, *Journal of Materials Chemistry A*, **6**, 17120 (2018).
114. S. W. Lee, W. Lee, Y. Hong, G. Lee, and D. S. Yoon, *Sensors Actuators B*, **255**, 1788 (2018).
115. S. Yu, D. Zhang, Y. Zhang, W. Pan, B. E. Meteku, F. Zhang, and J. Zeng, *Nanoscale*, **12**, 18815 (2020).
116. B. Cojocaru, D. Avram, V. Kessler, V. Parvulescu, G. Seisenbaeva, and C. Tiseanu, *Sci. Rep.*, **7**, 9598 (2017).
117. B. Sharma, J.-S. Sung, A. A. Kadam, and J. Myung, *Appl. Surf. Sci.*, **530**, 147272 (2020).
118. H.-J. Kim and J.-H. Lee, *Sensors Actuators B*, **192**, 607 (2014).
119. L. Zhang et al., *Sensors Actuators B*, **252**, 367 (2017).
120. A. A. Kadam, J.-S. Sung, and B. Sharma, *J. Alloys Compd.*, **854**, 157041 (2020).
121. X. Ren, T. Yan, D. Wu, R. Feng, and Q. Wei, *J. Mol. Liq.*, **198**, 388 (2014).

Review—A Pollutant Gas Sensor Based On Fe3 O4 Nanostructures: A Review

ORIGINALITY REPORT

4%	3%	5%	1%
SIMILARITY INDEX	INTERNET SOURCES	PUBLICATIONS	STUDENT PAPERS

PRIMARY SOURCES

1	"Handbook of Sol-Gel Science and Technology", Springer Science and Business Media LLC, 2018 Publication	1%
2	Muhamad Taufik Ulhakim, Muhammad Rezki, Kariana Kusuma Dewi, Syauqi Abdurrahman Abrori et al. "Review—Recent Trend on Two-Dimensional Metal-Organic Frameworks for Electrochemical Biosensor Application", Journal of The Electrochemical Society, 2020 Publication	1%
3	Submitted to University of California, Merced Student Paper	1%
4	"Functional Nanomaterials", Springer Science and Business Media LLC, 2020 Publication	1%
5	Ni Luh Wulan Septiani, Yusuf Valentino Kaneti, Brian Yuliarto, Nugraha et al. "Hybrid nanoarchitecturing of hierarchical zinc oxide wool-ball-like nanostructures with multi-	1%

walled carbon nanotubes for achieving sensitive and selective detection of sulfur dioxide", Sensors and Actuators B: Chemical, 2018
Publication

---

6 Nelson Pynadathu Rumjit, Paul Thomas, Chin Wei Lai, Yew Hoong Wong. "Review—Recent Advancements of ZnO/rGO Nanocomposites (NCs) for Electrochemical Gas Sensor Applications", Journal of the Electrochemical Society, 2021 1%
Publication

Exclude quotes	On	Exclude matches	< 1%
Exclude bibliography	On		

Review—A Pollutant Gas Sensor Based On Fe3 O4 Nanostructures: A Review

GRADEMARK REPORT

FINAL GRADE

/0

GENERAL COMMENTS

Instructor

PAGE 1

PAGE 2

PAGE 3

PAGE 4

PAGE 5

PAGE 6

PAGE 7

PAGE 8

PAGE 9

PAGE 10

PAGE 11

PAGE 12

PAGE 13